

**Ultra-high molecular weight complex coacervates via  
polymerization-induced electrostatic self-assembly**

Journal:	<i>Polymer Chemistry</i>
Manuscript ID	PY-COM-03-2024-000273.R1
Article Type:	Communication
Date Submitted by the Author:	28-Mar-2024
Complete List of Authors:	Rho, Julia; University of Birmingham School of Chemistry Korpusik, Angie; University of Florida, Hoteit, Miriam; University of Florida, Department of Chemistry Garrison, John; University of Florida, Department of Chemistry Sumerlin, Brent; University of Florida, Department of Chemistry;

## COMMUNICATION

## Ultra-high molecular weight complex coacervates via polymerization-induced electrostatic self-assembly

Julia Y. Rho,<sup>\*a</sup> Angie B. Korpusik,<sup>a</sup> Miriam Hoteit,<sup>a</sup> John B. Garrison,<sup>a</sup> Brent S. Sumerlin<sup>\*a</sup>

Received 00th January 20xx,  
Accepted 00th January 20xx

DOI: 10.1039/x0xx00000x

Advances in reversible-deactivation radical polymerization (RDRP), particularly the recent renaissance of photoiniferter polymerization, have led to new methods to achieve ultra-high molecular weight polymers with high functional-group tolerance. Utilizing these advances, we report the synthesis of ultra-high molecular weight charged polymers to generate micron-sized complex coacervates via photoiniferter-mediated polymerization. This method allows access to self-assembled polymeric nanostructures on a previously under-explored size regime. We also demonstrated the *in situ* generation of micron-sized self-assembled particles *via* polymerization induced-electrostatic self-assembly (PIESA).

### Introduction

The self-assembly of functional macromolecules is primarily governed by their functionality, size, composition, and dispersity. The ability to precisely tailor these parameters using reversible-deactivation radical polymerization (RDRP) techniques, such as reversible addition-fragmentation chain transfer (RAFT), has expanded access to well-defined polymeric nanomaterials. Polymers generated through RDRP have been widely adopted for various applications, from photocatalysis to drug/gene delivery.<sup>1-5</sup> Some critical reasons for the growth and popularity of these systems have been their ease of synthesis, high functional group tolerance, and the ability to control dispersity and generate various block copolymer (BCP) architectures.<sup>6</sup>

Many of the most commonly used motifs for polymer self-assembly are directly inspired by noncovalent interactions found in Nature, such as ionic interactions, hydrogen bonding, and the hydrophobic effect. Notably, the self-assembly of oppositely charged polymers to form complex coacervates has been employed to mimic the multiphase separation found throughout the intracellular environment. Complex coacervates can form through charge complexation of polyelectrolytes.<sup>7</sup> One method to achieve this is by designing a block copolymer that contains both a charged and non-charged block.<sup>8-11</sup> In an aqueous environment, oppositely charged polymers can interact to form complexes. Formation of an ion-rich core with a stabilizing non-charged corona block leads to liquid-liquid phase separation that can be exploited for nanoparticle formation. The ability to form block copolymers (BCP) that

contain both charged and non-charged segments has led to a library of hierarchical coacervate architectures, such as micelles, vesicles, crosslinked hydrogels, and hexagonal rods.<sup>9, 11-17</sup> However, the use of conventional block copolymers has limited the domain sizes of these assemblies to the nanoscale.

Conversely, Nature uses hierarchical assemblies across several length scales. On a microscopic level, cells are often referred to as the smallest unit, or denominator, of life; however, each cell is home to a variety of proteins (on the nanoscopic level), which determine its structure and function. In order to synthesize BCP coacervate assemblies that extend into the micron scale, new methods to form ultra-high molecular weight block copolymers from charged monomers would be required.<sup>18, 19</sup> In 2017, our group reported a simple and catalyst-free photoiniferter method to produce well-controlled UHMW polymers via light-activated reversible-deactivation radical polymerization.<sup>18</sup> Due to the absence of an exogenous initiator that is typically used in the analogous RAFT process, along with conditions that lead to high viscosities to retard chain diffusion, the rate of termination can be dramatically reduced to enable access to ultra-high molecular weights ( $\sim 10^7$  g/mol) while maintaining a low dispersity and high livingness for future chain extensions. This radical-based polymerization is amenable to highly functional monomers, including charged monomers that can lead to polyelectrolytes. While the initial reports of this approach focused on aqueous polymerizations of acrylamides, the scope has since been expanded to include heterogeneous aqueous media and styrenic and (meth)acrylic monomers in organic solvents.<sup>19-21</sup>

Interestingly, the self-assembly of ultra-high molecular weight block copolymers in solution would enable access to synthetic micromorphologies. Cao *et al.* demonstrated the self-assembly of UHMW diblock copolymers in thin films to reveal domain sizes larger than 150 nm.<sup>22</sup> It was noted that solvent-vapor annealing was needed to enhance chain mobility and facilitate spherical nanostructure formation. This paradigm shift

<sup>a</sup> George & Josephine Butler Polymer Research Laboratory, Center for Macromolecular Science & Engineering, Department of Chemistry, University of Florida, Gainesville, Florida 32611, United States.

† Electronic Supplementary Information (ESI) available: [details of any supplementary information available should be included here]. See DOI: 10.1039/x0xx00000x

in size regime could also open new biological applications, as these assemblies would allow for the compartmentalization of larger hydrophilic biomacromolecules, such as proteins and antibodies. Related work in polymersomes has demonstrated how multicompartamental microstructures could pave the way to designing increasingly complex multicomponent synthetic cells.<sup>23-26</sup>

This work utilizes photoiniferter-mediated polymerization to synthesize UHMW charged diblock copolymers. The resulting self-assembly of these polymers enables the formation of complex coacervates on the micron-size regime, pushing the limits of traditional micellar morphologies. Previously, Cai and co-workers have utilized the functional group tolerance of this radical-based polymerization method to observe in-situ nanoparticle formation by polymerization-induced electrostatic self-assembly (PIESA).<sup>27-29</sup> In this work, we leverage the ability of photoiniferter polymerization to readily achieve UHMWs to demonstrate the synthesis of micron-sized self-assembled complex coacervates. This method produces diblock copolymers with both neutral and charged segments that can create coacervates with liquid-liquid phase-separated regions. Additionally, the synthesis of ABC triblock copolymers, encompassing uncharged, anionic, and cationic segments, results in the spontaneous formation of micron-sized self-assembled structures.

## Results and Discussion

To achieve UHMW complex coacervates, we first sought the synthesis of diblock copolymers, that contained both charged and non-charged segments. As reported by Carmean *et al.*, to

grow the UHMW polymers in a controlled manner and retain high livingness for further chain extension, the rates of propagation and reversible termination need to be maximized while irreversible termination is kept to a minimum.<sup>18</sup> For this reason, photoiniferter polymerization was utilized to synthesize a neutral hydrophilic poly(*N,N*-dimethylacrylamide) (PDMA) macro-chain transfer agent (macroCTA), targeting a molecular weight of 1 MDa, which would make up the corona of the micelle. A molar ratio of [*N,N*-dimethylacrylamide (DMA)]:[CTA] = 10,100:1 was used to obtain a PDMA with a targeted number-average degree of polymerization (DP) of 10,100.

Cationic and anionic blocks were then installed via chain extension of the PDMA macroCTA with the charged monomers trimethylammonium ethyl acrylate (TMAEA) or 2-acrylamido-2-methylpropane sulfonic acid (AMPS) (Figure 1). Conversion of the monomer was monitored using <sup>1</sup>H NMR spectroscopy and size-exclusion chromatography (SEC) (Figures S3 and S4). All polymerizations were driven to high conversion (>97%) (SI). However, upon purification via dialysis, the hydrodynamic radius of the resuspended polymer showed an increase for both diblock polymers upon chain extension. In Figure 1 (and S6), the Z-average diameter from dynamic light scattering (DLS) of the PDMA macroCTA was 37 nm which, upon chain extension with AMPS and TMAEA, increased to 49 and 52 nm, respectively. The resulting ultra-high molecular charged diblock copolymers were then dissolved separately in water containing 0.4 M potassium bromide (see SI for details).<sup>9</sup> Upon mixing PDMA-*b*-PAMPS and PDMA-*b*-PTMAEA, spherical micelle formation through electrostatic interactions was observed via DLS and transmission electron microscopy (TEM) (Figure 2). These results are consistent with self-assembly of UHMW polymers

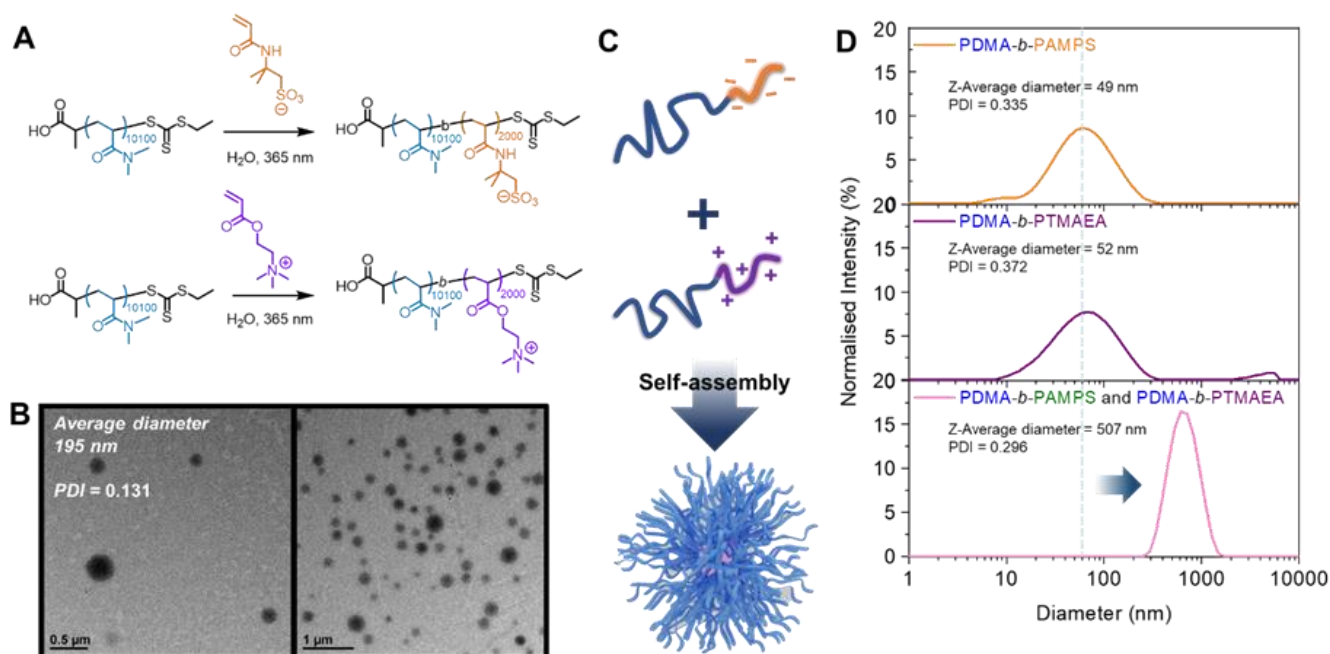


**Figure 1.** (a) General synthetic scheme for the chain extension of PDMA with TMAEA and AMPS, respectively, using photoiniferter polymerization (UV irradiation at 365 nm). (b) Transmission electron microscopy images of self-assembled ultra-high molecular weight charged diblock copolymers that form large complex coacervates via electrostatic interactions. (c) Schematic representation of ultra-high molecular weight charged polymers assembled to form micron-sized complex coacervates. (d) Dynamic light scattering of PDMA-*b*-PAMPS, PDMA-*b*-PTMAEA, and the co-assembly of PDMA-*b*-PAMPS and PDMA-*b*-PTMAEA.

that phase separate to form liquid-liquid domains in aqueous conditions via electrostatic interactions on the micron scale. Notably, the charged diblock copolymers showed a significant increase in hydrodynamic radius upon mixing from 49 (PDMA-*b*-PAMPS) and 52 nm (PDMA-*b*-PTMAEA) to 507 nm (PDMA-*b*-PAMPS + PDMA-*b*-PTMAEA). The resulting self-assemblies were confirmed to be spherical by TEM (Figure 2). The average diameter and polydispersity index (PDI) calculated via TEM were 195 nm and 0.131, respectively. As expected, the sizes determined by DLS are larger than those observed by TEM, as the ex-situ samples are taken in solution for DLS and the dry state for TEM. In addition, the solvated diffuse PDMA corona is expected to have a lower contrast compared to the high electron density found at the core of the assembly from the charged complexation of the anionic and cationic blocks.<sup>30</sup>

### Polymerization-induced electrostatic self-assembly of ultrahigh molecular weight polymers (UHMW PIESA)

Polymerization-induced self-assembly (PISA) has become one of the most widely used methods to generate polymer-based nanoparticles. The method relies on building a solvophilic polymeric chain which can be further chain extended using a solvophilic monomer that becomes, upon polymerization, progressively solvophobic. The resulting block copolymers undergo self-assembly to form nanoparticles during propagation.<sup>31</sup> In 2016, Armes and co-workers showed that small-angle x-ray scattering (SAXS) experiments could monitor this in situ self-assembly process.<sup>32</sup> Following this, Brendel, Sakurai, and co-workers demonstrated the mechanism and kinetics of micelle formation (i.e., the onset of self-assembly) could be deconvoluted.<sup>33</sup> Previous work in our group has also

looked at following PISA using fluorescent probes and in-situ liquid-cell TEM.<sup>34, 35</sup>

The most common PISA example is the formation of core-shell nanostructures in water through the growth of a hydrophobic core block stabilized by a pre-formed hydrophilic corona block.<sup>36-38</sup> However, the driving force behind this assembly process and core formation are not limited to hydrophobicity. Electrostatics have also been used to induce self-assembly in situ.<sup>39, 40</sup> In this work, we investigated the coacervation of the block copolymers during the polymerization process through PIESA.<sup>40</sup> Previously, Cai and co-workers have extensively utilized PIESA via polyion complexation to produce a wide range of nanomorphologies.<sup>27, 28, 41-43</sup> Here, we designed an UHMW triblock copolymer (PDMA-*b*-PAMPS-*b*-PTMAEA) which would contain neutral, anionic, and cationic blocks that undergo electrostatically-induced self-assembly during polymerization. Charged anionic diblock copolymer (PDMA-*b*-PAMPS) was chain extended with TMAEA (cationic monomer). The conversion was followed by <sup>1</sup>H NMR spectroscopy, and the polymerization reached 26% conversion after 8 h. Due to the zwitterionic nature of the polymer and its propensity to self-assemble into micron-sized spherical nanoparticles in water, SEC was not attempted for this polymer.

The resulting self-assembled coacervates were studied via DLS and TEM (Figure 2). DLS showed that the self-assembled structure attributed to the triblock copolymer reached an average diameter of 2.3  $\mu\text{m}$  — a clear increase in the diameter from the diblock macroCTA (49 nm, PDMA-*b*-PAMPS). In the TEM images, we also observed the formation of spherical particles with an average diameter of 313 nm. Importantly, this is the first demonstration of highly functional synthetic micromorphologies generated through photoinitiated PIESA.

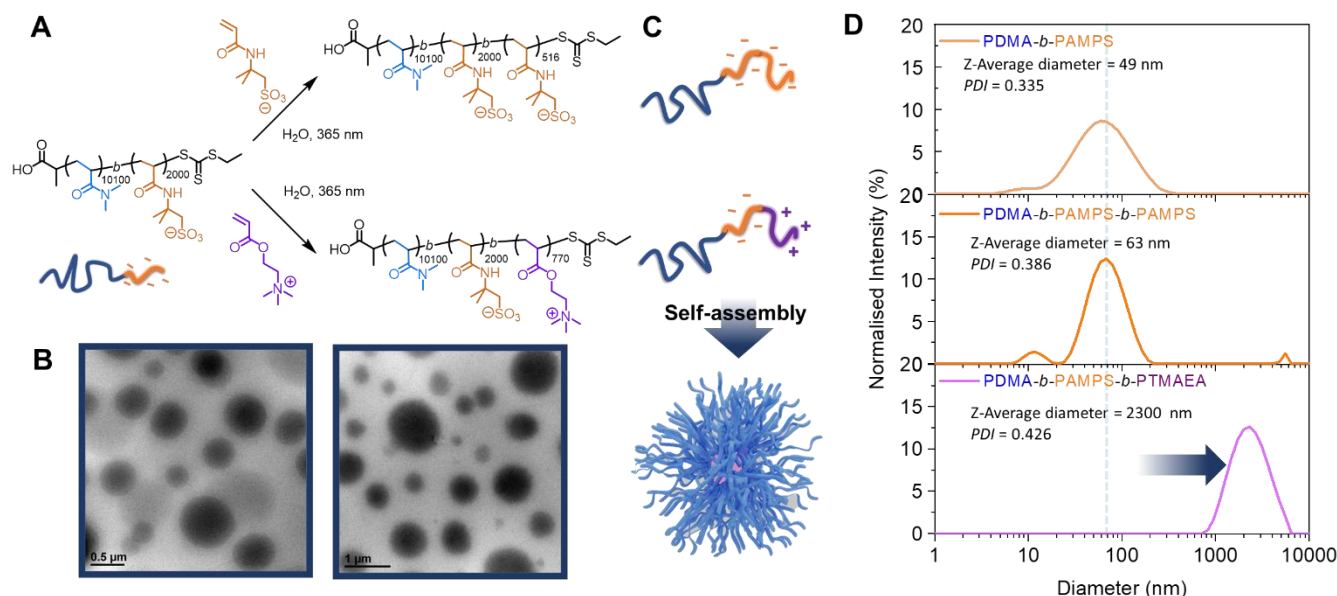


**Figure 2.** (a) General synthetic scheme for the chain extension of PDMA-*b*-PAMPS with TMAEA and AMPS, respectively, using photoiniferter polymerization (UV irradiation at 365 nm). (b) Transmission electron microscopy images and (c) Schematic representation of ultra-high molecular weight complex coacervates formed through polymerization-induced electrostatic self-assembly. (d) Dynamic light scattering of PDMA-*b*-PAMPS, PDMA-*b*-PAMPS-*b*-PAMPS, PDMA-*b*-PAMPS-*b*-PTMAEA.

The self-assembly of the PDMA-*b*-PAMPS chain extended with AMPS was studied as a control (conversion = 39% after 8 h). As predicted, a slight increase in the hydrodynamic volume of the polymer was observed from 49 (PDMA-*b*-PAMPS) to 63 nm (PDMA-*b*-PAMPS-*b*-PAMPS), but no significant increase associated with coacervate formation was observed.

Note that there is a disparity in the average diameter of the complex coacervates formed through the diblock and triblock systems (0.51  $\mu\text{m}$  and 2.3  $\mu\text{m}$ , respectively). This difference is likely due to charge compensation, as the triblock system has a shorter positive block than the diblock system. Additionally, the energetic barriers to forming these coacervates in situ versus mixing could also significantly affect the organization of the charged complexes. Achieving a narrower distribution of particles (i.e., lower dispersity) on this length scale could provide interesting new avenues for their application.

### Uniform micron-sized complex coacervates

Confocal laser scanning microscopy (CLSM) was used to study the size distribution of complex coacervates (formed by mixing PDMA-*b*-PAMPS and PDMA-*b*-PTMAEA). The resulting complex coacervates adopt a broad distribution of particle sizes, the average diameter of the particles being  $2.00 \pm 0.34 \mu\text{m}$ , similar to those observed previously in DLS, TEM, and literature, Figure 2.<sup>44</sup> Interestingly, upon vortexing the solution for 30 s, the resulting particles reduce in diameter and become

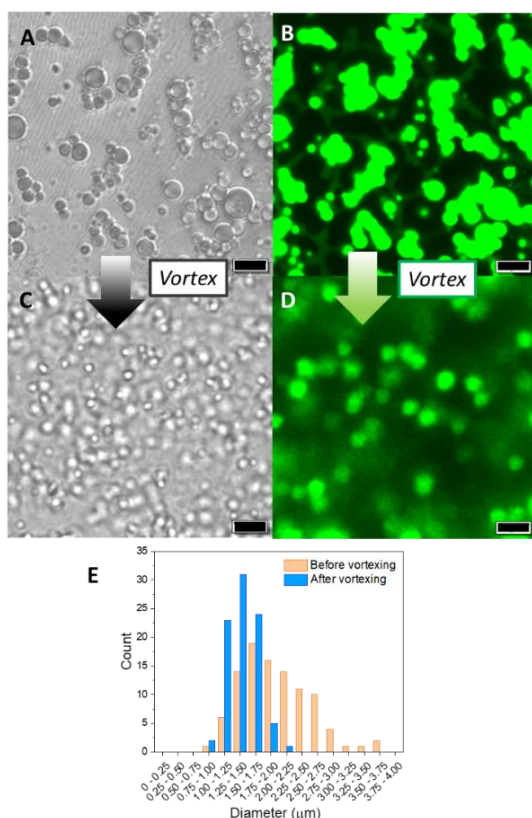


**Figure 3.** Confocal laser scanning microscopy of complex coacervates with fluorescein dye (PDMA-*b*-PAMPS and PDMA-*b*-PTMAEA), before (a,b) brightfield and fluorescence detector at 405 nm, and after vortexing (c,d) bright field and fluorescence detector at 405 nm. (e) Histogram of counting particle diameter.

more uniform ( $1.42 \pm 0.26 \mu\text{m}$ ). This uniformity can also be observed in fluorescence images (upon adding fluorescein) and the histogram of the particle diameters in Figure 3b-e. Therefore, utilizing low dispersity UHMW polymers allows us to generate low dispersity, uniform particles on the micron scale.

### Conclusion

In conclusion, we have demonstrated how the high livingness and functional group tolerance of photoiniferter polymerization could be used to produce ultra-high molecular weight complex coacervates. Importantly, this method generates non-charged and charged diblock copolymers that can form complex coacervates with liquid-liquid phase-separated domains. Furthermore, generating triblock copolymers containing neutral, anionic, and cationic blocks leads to the in-situ formation of micron-sized self-assembled structures. To our knowledge, this is the first example of synthetic micromorphologies generated through polymerization-induced self-assembly. This work pushes past limits in size regime and benefits from the precision and versatility of controlled radical polymerization techniques on the micron scale, analogous to complex microorganisms found in Nature. Building increasingly larger and more complex synthetic and responsive constructs, such as those explored in this work, could open potential avenues to exciting new biotechnologies.

### Conflicts of Interest

There are no conflicts to declare.

### Acknowledgments

The authors would like to acknowledge Dr. Georg M. Scheutz and Dr. Rebecca Olson for their scientific discussions throughout this project.

### References

1. K. Bunyamin, E. Lars, T. D. Hien, S. B. Johan, B. Cyrille and P. D. Thomas, *Polym. Chem.*, 2013, **5**, 350-355.
2. P. Gurnani and S. Perrier, *Prog. Polym. Sci.*, 2020, **102**, 101209.
3. H. Phan, V. Taresco, J. Penelle and B. Couturaud, *Biomater. Sci.*, 2021, **9**, 38-50.
4. R. Li, K. Landfester and C. T. J. Ferguson, *Angew. Chem. Int. Ed.*, 2022, **61**, e202211132.
5. M. G. Hanson, C. J. Grimme, C. F. Santa Chalarca and T. M. Reineke, *Bioconjug. Chem.*, 2022, **33**, 2121-2131.
6. J. K. Daniel, *Chem. Soc. Rev.*, 2013, **43**, 496-505.
7. J. T. G. Overbeek and M. J. Voorn, *J. Cell. Physiol.*, 1957, **49**, 7-26.
8. D. V. Krogstad, S.-H. Choi, N. A. Lynd, D. J. Audus, S. L. Perry, J. D. Gopez, C. J. Hawker, E. J. Kramer and M. Tirrell, *J. Phys. Chem. B*, 2014, **118**, 13011-13018.

9. Y. Liu, C. F. S. Chalarca, R. N. Carmean, R. A. Olson, J. Madinya, B. S. Sumerlin, C. E. Sing, T. Emrick and S. L. Perry, *Macromolecules*, 2020, **53**, 7851-7864.
10. C. E. Sing and S. L. Perry, *Soft Matter*, 2020, **16**, 2885-2914.
11. J. N. Hunt, K. E. Feldman, N. A. Lynd, J. Deek, L. M. Campos, J. M. Spruell, B. M. Hernandez, E. J. Kramer and C. J. Hawker, *Adv. Mater.*, 2011, **23**, 2327-2331.
12. W. C. Blocher and S. L. Perry, *Wiley Interdiscip. Rev. Nanomed. Nanobiotechnol.*, 2017, **9**, e1442.
13. I. K. Voets, A. de Keizer and M. A. Cohen Stuart, *Adv. Colloid Interface Sci.*, 2009, **147-148**, 300-318.
14. H. M. van der Kooij, E. Spruijt, I. K. Voets, R. Fokkink, M. A. Cohen Stuart and J. van der Gucht, *Langmuir*, 2012, **28**, 14180-14191.
15. C. Li, B. G. P. van Ravensteijn, M. A. C. Stuart, J. R. Magana and I. K. Voets, *Macromol. Chem. Phys.*, 2022, **223**, 2200195.
16. C. C. M. Sproncken, B. Gumí-Audenis, S. Foroutanparsa, J. R. Magana and I. K. Voets, *Macromolecules*, 2023, **56**, 226-233.
17. A. E. Marras, J. M. Ting, K. C. Stevens and M. V. Tirrell, *J. Phys. Chem. B*, 2021, **125**, 7076-7089.
18. R. N. Carmean, T. E. Becker, M. B. Sims and B. S. Sumerlin, *Chem*, 2017, **2**, 93-101.
19. R. N. Carmean, M. B. Sims, C. A. Figg, P. J. Hurst, J. P. Patterson and B. S. Sumerlin, *ACS Macro. Lett.*, 2020, **9**, 613-618.
20. R. A. Olson, M. E. Lott, J. B. Garrison, C. L. G. Davidson, L. Trachsel, D. I. Pedro, W. G. Sawyer and B. S. Sumerlin, *Macromolecules*, 2022, **55**, 8451-8460.
21. C. L. G. I. V. Davidson, M. E. Lott, L. Trachsel, A. J. Wong, R. A. Olson, D. I. Pedro, W. G. Sawyer and B. S. Sumerlin, *ACS Macro Letters*, 2023, **12**, 1224-1230.
22. W. Cao, S. Xia, M. Appold, N. Saxena, L. Bießmann, S. Grott, N. Li, M. Gallei, S. Bernstorff and P. Müller-Buschbaum, *Sci. Rep.*, 2019, **9**, 18269.
23. K. T. Kim, J. J. L. M. Cornelissen, R. J. M. Nolte and J. C. M. van Hest, *Adv. Mater.*, 2009, **21**, 2787-2791.
24. N. P. Kamat, J. S. Katz and D. A. Hammer, *J. Phys. Chem. Lett.*, 2011, **2**, 1612-1623.
25. R. J. R. W. Peters, M. Marguet, S. Marais, M. W. Fraaije, J. C. M. v. Hest and S. Lecommandoux, *Angew. Chem. Int. Ed.*, 2014, **53**, 146-150.
26. H. Che and J. C. M. van Hest, *Chemnanomat*, 2019, **5**, 1092-1109.
27. Q. Zhao, Q. Liu, C. Li, L. Cao, L. Ma, X. Wang and Y. Cai, *Chem. Commun.*, 2020, **56**, 4954-4957.
28. W. Xiong, X. Wang, Y. Liu, C. Luo, X. Lu and Y. Cai, *Macromolecules*, 2022, **55**, 7003-7012.
29. L. Wang, Y. Ding, Q. Liu, Q. Zhao, X. Dai, X. Lu and Y. Cai, *ACS Macro. Lett.*, 2019, **8**, 623-628.
30. K. C. Stevens, A. E. Marras, T. R. Campagna, J. M. Ting and M. V. Tirrell, *Macromolecules*, 2023, **56**, 5557-5566.
31. A. B. Korpusik, Y. Tan, J. B. Garrison, W. Tan and B. S. Sumerlin, *Macromolecules*, 2021, **54**, 7354-7363.
32. M. J. Derry, L. Fielding, A. , N. J. Warren, C. J. Mable, A. J. Smith, O. O. Mykhaylyk and S. P. Armes, *Chem. Sci.*, 2016, **7**, 5078-5090.
33. R. Takahashi, S. Miwa, F. H. Sobotta, J. H. Lee, S. Fujii, N. Ohta, J. C. Brendel and K. Sakurai, *Polym. Chem.*, 2020, **11**, 1514-1524.
34. J. Y. Rho, G. M. Scheutz, S. Häkkinen, J. B. Garrison, Q. Song, J. Yang, R. Richardson, S. Perrier and B. S. Sumerlin, *Polym. Chem.*, 2021, **12**, 3947-3952.
35. G. M. Scheutz, M. A. Touve, A. S. Carlini, J. B. Garrison, K. Gnanasekaran, B. S. Sumerlin and N. C. Gianneschi, *Matter*, 2021, **4**, 722-736.
36. A. Blanazs, A. J. Ryan and S. P. Armes, *Macromolecules*, 2012, **45**, 5099-5107.
37. L. P. D. Ratcliffe, A. J. Ryan and S. P. Armes, *Macromolecules*, 2013, **46**, 769-777.
38. G. M. Scheutz, J. I. Bowman, S. Mondal, J. Y. Rho, J. B. Garrison, J. Korpanty, N. C. Gianneschi and B. S. Sumerlin, *ACS Macro Letters*, 2023, **12**, 454-461.
39. A. C. Figg, A. Simula, K. A. Gebre, B. S. Tucker, D. M. Haddleton and B. S. Sumerlin, *Chem. Sci.*, 2014, **6**, 1230-1236.
40. Y. Ding, Q. Zhao, L. Wang, L. Huang, Q. Liu, X. Lu and Y. Cai, *ACS Macro. Lett.*, 2019, **8**, 943-946.
41. J. Yanyan, X. Na, H. Jie, Y. Qiuping, G. Lei, G. Pan, L. Xinhua and C. Yuanli, *Polym. Chem.*, 2015, **6**, 4955-4965.
42. M. Cai, Y. Ding, L. Wang, L. Huang, X. Lu and Y. Cai, *ACS Macro. Lett.*, 2018, **7**, 208-212.
43. Q. Liu, X. Wang, L. Ma, K. Yu, W. Xiong, X. Lu and Y. Cai, *ACS Macro. Lett.*, 2020, **9**, 454-458.
44. S. Gao and S. Srivastava, *ACS Macro. Lett.*, 2022, **11**, 902-909.